南通大學

外 文 翻 译

学　　生：_____张壮壮_____

专　　业：_____物联网工程_____

指导教师：_____王　进_____

An intelligent machine vision-based smartphone app for beef quality Evaluation

Soleiman Hosseinpour ∗ , Ali Hakimi Ilkhchi, Mortaza Aghbashlo

Nanobioelectronics Lab., Department of Mechanical Engineering of Agricultural Machinery, Faculty of Agricultural Engineering and Technology, College of Agriculture and Natural Resources, University of Tehran, Karaj, Iran

Beef tenderness is the most important attribute correlated with beef quality, consumer satisfaction, and purchasing decisions. Nowadays, a rapid, non-invasive, and non-destructive evaluation and prediction of beef tenderness and quality from fresh product attributes is desired in industries, laboratories, and markets dealing with beef handling, processing, analyzing, and buy and sell. In this study, a new machine vision-based smartphone app was developed and verified for the first time in order to predict beef tenderness from fresh beef image captured under uncontrolled conditions. In order to eliminate the effects of uncontrolled imaging conditions, an illumination-, rotation-, scale-, and translation-invariant image processing algorithm was developed so that a common user can easily capture the image of the beef sample with more degree of freedom in terms of luminance, rotation, scale, and translation with no worries about the accuracy of the results. The obtained preprocessed image textural features were well correlated with instrumental data obtained using Warner Bratzler shear force measurement through artificial neural network technique. The developed android app was installed on a LG G4 H815 smartphone and its performance was assessed using thirty unseen beef samples. The probability of occurrence of 2-D correlation coefficients obtained from the analyses of all the beef samples subjected to the image processing algorithm showed the average probability of 0.92, which strongly supported the robustness of the developed algorithm. The best obtained neural network model could predict the tenderness values with mean absolute percentage error (MAPE) of 3.28% and coefficient of determination (R^2) of 0.97. The app promisingly predicted the beef tenderness values of the unseen samples with mean squared error (MSE) of 3.34, MAPE of 3.74%, and R^2 of 0.99. Accordingly, the developed app can be a low-cost and user-friendly tool for predicting beef tenderness and quality from its real-world image.

1. Introduction

Beef eating quality and palatability attributes are mostly characterized by tenderness (texture), juiciness, and flavor (Aaslyng, 2002).These sensory properties are important for customer satisfaction and making purchasing decisions (Platter et al., 2005). In the case of quality, tenderness is one of the most important attributes regarding sensory experience and eating satisfaction. According to Platter et al. (2005), consumers are willing to pay more for tender beef products. Tenderness is evaluated by objective and subjective methods like Warner Bratzler shear force (WBSF) and consumer panel, respectively (Destefanis et al., 2008), but, the majority of these methods are invasive and destructive assessment approaches and need sample preparation. Several relatively new methods like visible, hyperspectral imaging (ElMasry et al., 2012), spectroscopy (Bowling et al., 2009), ultrasonic technology (Tait, 2016), and X-ray computed tomography (Prieto et al., 2010) have been developed and used for beef tenderness prediction; however, most of these methods are not cost-effective and need sophisticated instruments.

In meat industry, a rapid, non-invasive, and non-destructive evaluation and prediction of meat quality from fresh product attributes is desired. Machine (computer) vision technology is a powerful and widely used tool for food quality inspection because of being reliable, robust, cost-effective, non-invasive, and non-destructive (Hosseinpour et al., 2014). Therefore, numerous researches have been devoted in the literature where image processing technique has been used to predict the beef quality (Li et al., 2001; Jackman et al., 2010). Beef image features like color, marbling, and texture can excellently reflect the beef quality (Xiong et al., 2014). Notably, surface image texture associated with connective tissue contents and fiber bundle size in beef mussel is an important indicator of beef tenderness (Swatland, 2006; Jabri et al.,2010).

Nomenclature		R_i	RGB channels (i = 1, 2, 3)
		$S(\lambda)$	surface reflectivity
A, B	Invariant images	T	score vector
$\bar{A}, \bar{B}$	average of the intensities in invariant images	W	matrix of weights
a^x	direction of the light source	X	standardized textural features vector
$E(\lambda)$	spectral power distribution	x	location on the image plane
$F(\lambda)$	spectral sensitivity	λ	wavelength (nm)
I	intensity	μ	mean
N_g	number of gray levels	σ^2	variance
n^x	surface normal vector	σ_i, σ_j	standard deviations (i = 0, 1, ..., (N_g-1)), (j = 0, 1, ...,
p_d	normalized symmetric GLCM ($N_g \times N_g$)		(N_g-1))
R	image sensor response		

Human-smartphone interactions are growing day-by-day and affecting many aspects of our lives. Smartphones are the forerunner generations of cell phones equipped with powerful processors, built-in sensors, larger storage, wireless communications, and standard open source software, enabling them to sense and understand their environment. Accordingly, smartphones have created new research op portunities to design and implement android apps in many domains such as healthcare (Higgins, J.P., 2016; Jacobs et al., 2017), medical and biotechnology (Zhang et al., 2016; Liao et al., 2016), agriculture(Han et al., 2016; Vesali et al., 2015), food industry (Yu et al., 2015;Masawat et al., 2105), medicine (Bueno et al., 2016; Cho et al., 2015),environmental monitoring, biosecurity and bioterrorism (Hutchison et al., 2015), tourism (Law et al., 2018), and internet of things (Fitzgerald et al., 2018).

In recent years, there has been a growing interest among researchers to develop image processing applications using smartphone's camera (Chung et al., 2018; Shrivastava et al., 2018). This could be attributed to the fact that the cost of smartphones is low, while their processing capabilities are enhanced thanks to the advanced processors, high-resolution cameras, and memory storage devices. Even though smartphone-based vision has created new applications in image processing and artificial intelligence, there are still many challenges to be addressed before the commercialization of such android apps. Various influential parameters like illumination, viewpoint (rotation, scaling, and translation), camera parameters (aperture, shutter speed, white balance, focus, and ISO), and hardware limitations and diversity can profoundly affect the performance, accuracy, and complexity of the smartphone-based vision systems. In order to address these issues, various approaches have been developed and employed like imaging under controlled conditions (Choodum et al., 2013) and using advanced image processing algorithms (Casanova et al., 2013). However, it is difficult or even impossible to control the imaging environment in smartphone applications. Invariant features extraction is still a key challenge in pattern recognition and image processing. Accordingly, several image processing algorithms have been developed to extract invariant features from images captured under uncontrolled conditions in order to improve the performance of vision systems (Legaz et al., 2018; Zhu et al., 2017), but the developed algorithms have rarely been used in smartphone-based image processing (Casanova et al., 2013).

Therefore, this study was conducted for the first time to create a new smartphone app on the basis of fresh beef image captured under non-standardized and uncontrolled conditions for estimating tenderness (WBSF value) of the fresh beef sample. To this end, an illumination-, rotation-, scale-, and translation-invariant image processing algorithm was developed for the first time to extract invariant image texture features from fresh beef images. The obtained features were then correlated with Warner Bratzler shear force (WBSF) data using a machine learning technique namely artificial neural network (ANN) model. The algorithm was used to build a user-friendly smartphone app for real-time prediction of beef tenderness under real-world imaging conditions and afterwards, the prediction accuracy of the app was confirmed using thirty unseen meat samples. Using this app, consumers will be able to predict the required force for chewing the beef intended for buy just at the time of purchase. Finally, the developed app has a great potential to be applied in markets by common consumers and in laboratories and meat industries by specialists for evaluating beef quality.

2. Materials and methods

2.1. Samples preparation

The muscle samples of 167 carcasses were taken from a local butcher shop. The M. longissimus dorsi muscles of the all carcasses were removed in the store. All the muscle samples were divided into two groups including 137 and 30 carcasses as the training and testing samples, respectively. To carry out experiments, 2.5-cm-thick steak samples were taken from 12th/13th rib interface over the longitudinal direction of the muscle. Therefore, the surface of the beef samples was smooth as much as possible. The fresh samples were used in experiments immediately without storage. First, the required images were taken from beef samples by smartphone. The samples were then broiled to measure the meat tenderness using WBSF standard according to the research guidelines for cookery methods as prescribed by American Meat Science Association (AMSA, 2005).

2.2 Image acquisition

A LG G4 H815 smartphone with high resolution CCD sensor camera (5312 × 2988 pixels, 1/2.6″ inches, f/1.8) was used to capture the fresh beef images. The images with resolution of 2976 ×2976 pixels were captured intentionally under different conditions in terms of illumination, rotation, distance, and translation between the camera and the sample planes. The images were captured without any background (close up images) from the samples. The close up image does not require any preprocessing steps because the entire image is the region of interest.

2.3 Features extraction

Since there exist positional and lighting variations during image acquisition with smartphones, illumination- and affine-invariant (i.e., translation-, rotation- and scale-invariant) methods should be applied to remove the effects of such uncontrolled conditions and to extract robust textural features. The invariant feature extraction algorithm proposed herein consists of three subroutines including illumination invariant, affine invariant, and textural features extraction algorithms. The overall feature extraction procedure can be divided into the following steps:

i) the captured color images were resized to 25% of the original size (resized to 744 ×744 pixels) to increase time efficiency of the algorithms,

ii) median filter (3 × 3) was employed to eliminate the environmental noises from the images as well as salt and pepper noises which can be caused by sharp and unforeseen disturbances in the image due to, for example, some defects in the CCD or in the transmission of the image. The mechanism of the median filter is to run through the image array by array, replacing each entry with the median of neighboring arrays,

iii) color images were converted from RGB space to the illumination invariant gray level space,

iv) the translation-, rotation-, and scale-invariant space were derived from the illumination-invariant gray level space, and

v) the textural features were extracted from the last obtained space.

2.3.1. Illumination-invariant space

Illumination-invariant color space was achieved using the method proposed by Maddern et al. (2014). This invariant space is extracted from the camera response function, showing the response of an image sensor R with a spectral sensitivity function F(λ) to the light I reflected from a scene with surface reflectivity S(λ) under illumination source with spectral power distribution E(λ) as follows:

$$R^{x,E} = a^x \cdot n^x \, I^x \int S^x(\lambda). \; E^x(\lambda). \; F(\lambda) \, d\lambda \tag{1}$$

where a^x and n^x represent the direction of the light source and the surface normal vector, respectively (Fig. 1). By modeling the spectral sensitivity function as a Dirac delta function and separating the components of Eq. (1) using logarithmic transform, the camera response function simply changes to the following equation:

$$\log(R^{x,\,E}) = \log\{G^x I^x\} + \log\{S^{\,x}(\lambda_i)\} + \log\{E^x(\lambda_i)\} \tag{2}$$

where G is a^n ·x^x called the geometry factor. Maddern et al. (2014) extracted one-dimensional gray level space I from Eq. (2) as follows:

$$I = \log(R_2) - \alpha \log(R_1) - (1 - \alpha)\log(R_3) \tag{3}$$

where R1 , R2 , R3 are the sensor responses in the three RGB channels. The α value is determined by having the values of the three wavelengths corresponding to the peak of sensitivities (λ 1 < λ 2 < λ 3) as follows:

$$\frac{1}{\lambda_2} = \frac{\alpha}{\lambda_1} + \frac{(1-\alpha)}{\lambda_3} \tag{4}$$

In order to determine the α value and, consequently, illumination invariant gray level space, peak values of the sensor spectral responses are required. Fig. 2 shows the details of the procedure used for deriving illumination-invariant gray level space from an image in the RGB color space.

2.3.2. Rotation-, scale-, and translation-invariant space

To achieve a rotation-, scale-, and translation-invariant space, Fourier-Mellin transform was applied to the obtained illumination-invariant gray level space. As illustrated in Fig. 3, Rotation-, scale-, and translation-invariant algorithm is composed of three successive transforms including Fourier transform, log-polar transform, and Fourier transform. The log-polar transform is the most popular Coordinate transformation (Asselin and Arsenault, 1994), mapping rotation and scale to translation because of its topological nature. On the other hand, translation-, rotation-, and scale-invariant space can be achieved based on the shift theorem of the Fourier transform. Fourier shift theorem states that a translation in the spatial domain corresponds to a linear phase term in the frequency domain.

To investigate the robustness of the developed image processing algorithm, the image capturing procedure of each beef sample was performed in three levels of luminance (400, 700, and 1000 lx) three levels of rotation (0°, 45°, and 90°), three levels of scale (0.5, 0.8, and 1), three levels of translation (0, 25, and 50% of the image width) in each horizontal and vertical direction in the image plane, and three replications. Then, robustness of the image processing algorithm was measured via 2-D correlation coefficient (Eq. (5)) of each pair of images for each beef sample captured in different conditions in terms of illumination, rotation, scale, and translation.

$$r = \frac{\sum_m \sum_n (A_{mn} - \bar{A})(B_{mn} - \bar{B})}{\sqrt{(\sum_m \sum_n (A_{mn} - \bar{A})^2)(\sum_m \sum_n (B_{mn} - \bar{B})^2)}} \qquad (5)$$

where, $\bar{A}$ and $\bar{B}$ are respectively the average of the intensities in images A and B in the illumination-, rotation-, scale-, and translation-invariant space. Finally, statistical analysis was performed using MATLAB software (Release, 2016b) to find the effect of replications on the 2-D correlation coefficients.

2.3.3. Texture features

Gray level co-occurrence matrix (GLCM) is the most popular and the first statistical method used for analyzing texture of food images (Zheng et al., 2006). A GLCM is a probability distribution matrix derived based on second-order statistical technique presented by Haralick and Shanmugam (1973). The widely used GLCM technique was considered in this study for extracting image textural features. Various textural features such as variance, correlation, homogeneity, energy, entropy, sum entropy, and sum variance (Eqs. (6)–(12)) and some statistical features such as mean, variance, and entropy were respectively extracted from the amplitude and real parts of the normalized GLCM of the obtained illumination- and affine-invariant space for encoding the randomness, linearity among pixels, pixel similarity, and textural uniformity of the space:
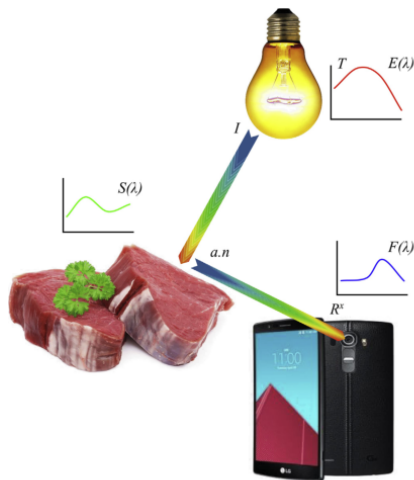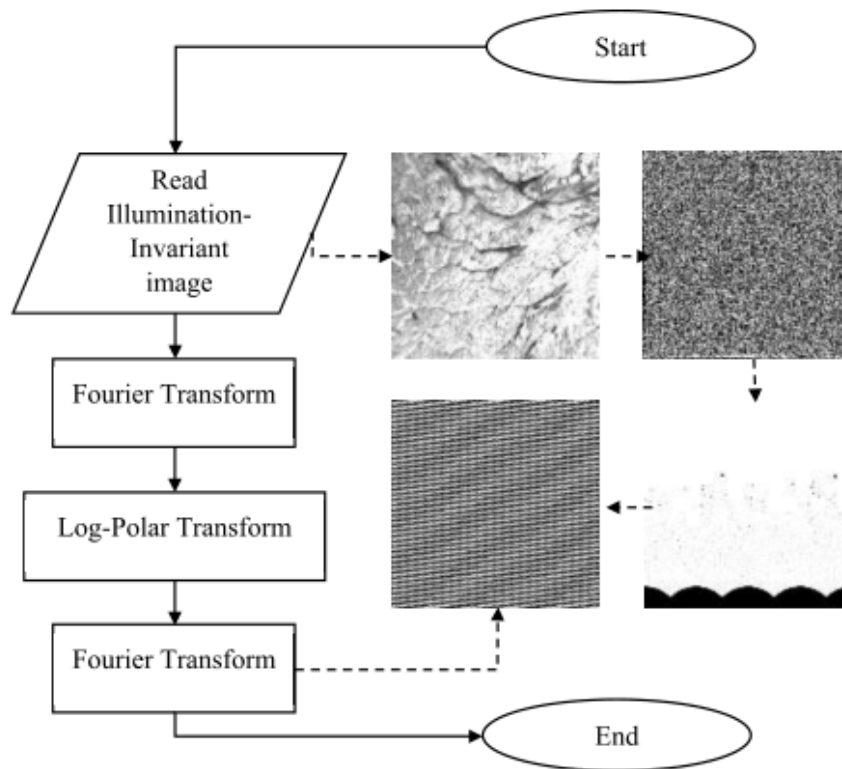

Fig. 1. Camera response function and its components.

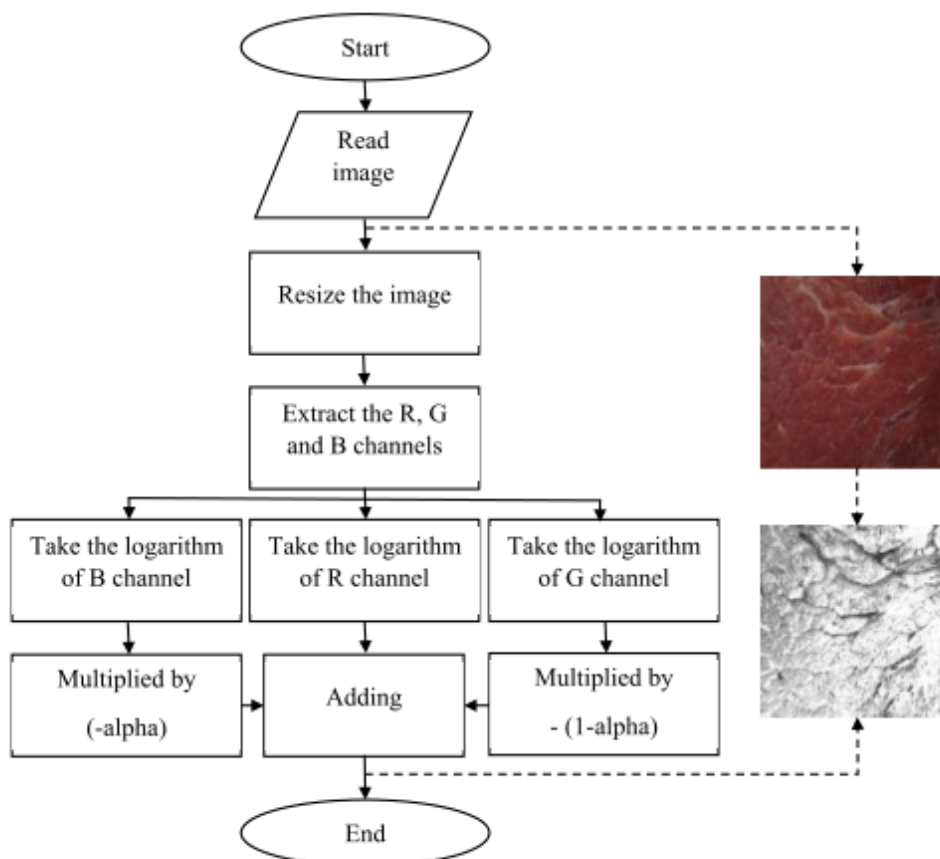**Fig. 3.** Rotation-, Scale- and translation-invariant sub-algorithm flowchart.

Fig. 2. Illumination-invariant subroutine flowchart.

(a)

(b)

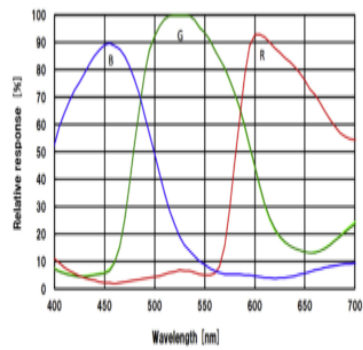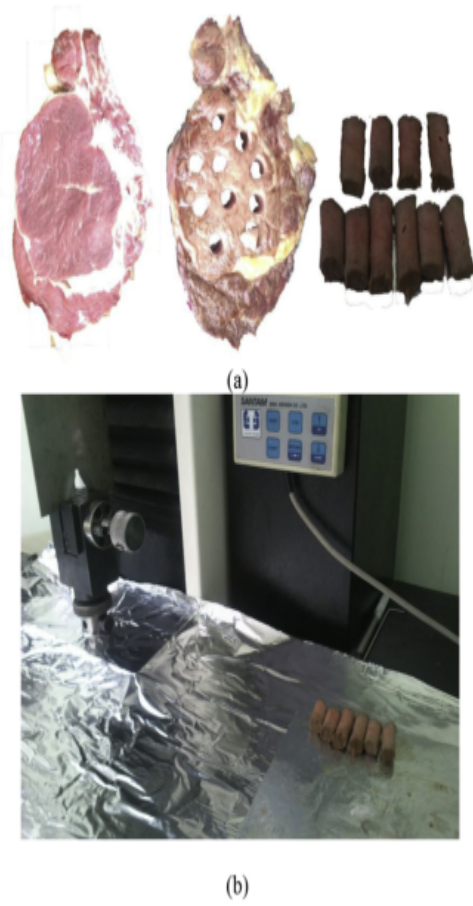**Fig. 5.** Flowchart of the proposed algorithm for the app.

Fig. 6. Wavelength sensitivities of the camera sensor to R, G, and B channels.

8

(c)

Table 1

Peak sensitivities at ordered wavelengths ($\lambda_1 < \lambda_2 < \lambda_3$) and their alpha value.

Camera	Image sensor	λ_1 (nm)	λ_2 (nm)	λ_3 (nm)	α
LG-H850	Sony- IMX234	454.74	524.77	602.75	0.4572

$$\sigma^2 = \sum_{i=0}^{Ng-1} (i - \mu)^2 p_d \tag{6}$$

$$Correlation = \frac{\sum_{i=1}^{Ng} \sum_{j=1}^{Ng} (i - \mu_i)\, p_d(i,j)}{\sigma_i\, \sigma_j} \tag{7}$$

$$Homogeneity = \sum_{i=1}^{Ng} \sum_{j=1}^{Ng} \frac{p_d(i,j)}{1 + |i-j|} \tag{8}$$

$$Energy = -\sum_{i=0}^{Ng} \sum_{j=0}^{Ng} p_d^2(i,j) \tag{9}$$

$$Entropy = -\sum_{i=0}^{Ng} \sum_{j=0}^{Ng} p_d(i,j)\, log\left(p_d(i,j)\right) \tag{10}$$

$$Sum\ Entropy = -\sum_{i=0}^{2(Ng-1)} p_d(i)\, log\left(p_d(i)\right) \tag{11}$$

$$Sum\ Variance = -\sum_{i=0}^{2(Ng-1)} (i - Sum\ of\ Entropy)^2\, p_d(i) \tag{12}$$

2.4. Tenderness measurement

To measure the tenderness of the beef samples, the well-known Warner-Bratzler shear force (WBSF) method was used. This method measures the cutting shear force as the mechanical property of the cooked meat. The measurements were performed on an Instron Machine (Santam STM-5 Instron Material Testing Machine) equipped with a Warner-Bratzler cutting device. All samples were prepared according to the American Meat Science Association guidelines (AMSA, 2005) for the WBSF and sensory measurements. The prepared samples were cooked in an electric oven (Bakers Pride P22S). The temperature of the oven was set at 177°C for both of the top and bottom heating plates. The internal temperature of the beef sample was measured and controlled at their center by a digital thermometer containing a temperature sensor (DS18b20, 55–125°C) inserted into the geometric center of the sample and an Arduino microcontroller. When the peak internal temperature of the samples reached to 71 °C, the beef samples were removed from the oven and allowed to reach the ambient temperature (22 °C). It is worthy to note that the samples were turned once during the broiling procedure when the internal temperature reached half the increase to the final internal temperature. Six or ten cores having 1.27cm diameter were obtained parallel to the muscle fiber orientation from different locations of each sample (Fig. 4(a)). It should be noted that the sampled locations were already imaged. All the prepared core samples were exposed to shear force perpendicular to the muscle fiber direction by the Instron material testing machine. The crosshead speed of shear blade was set at 200 mm/min (AMSA, 2005). Peak shear force (in Newton) was considered as the tenderness indicator parameter and recorded for each core sample (Fig. 4(b and c)).
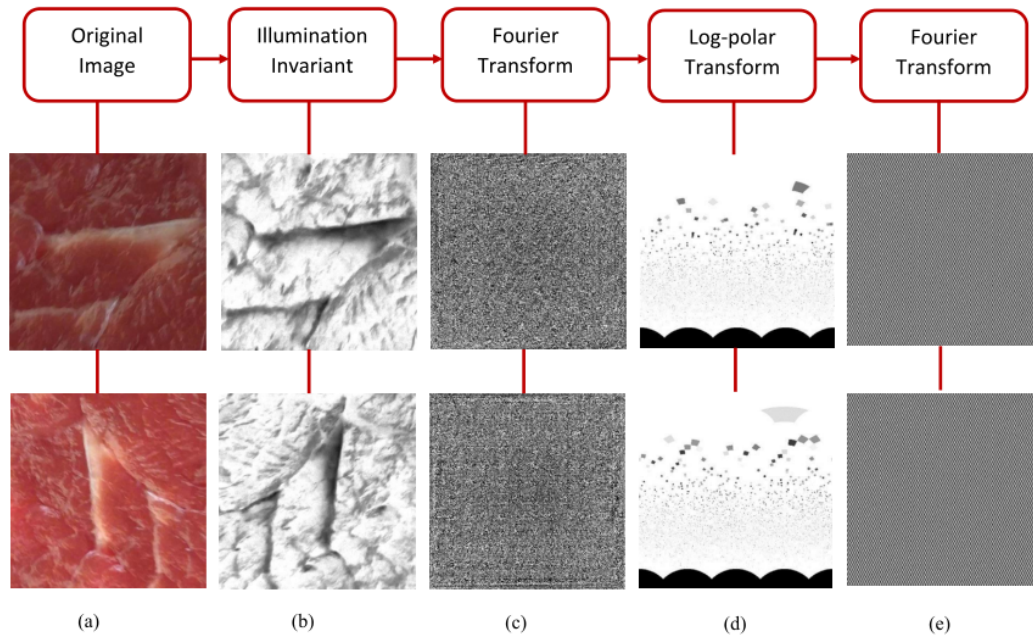
Table 2

2-D correlation coefficients of the obtained images via the developed image processing algorithm for a beef sample under imaging at a constant level of translation (0% of the image width), three levels of rotation (r_0, r_1, and r_2), and three levels of scale (s_0, s_1, and s_2), three levels of luminance (l_0, l_1, and l_2).

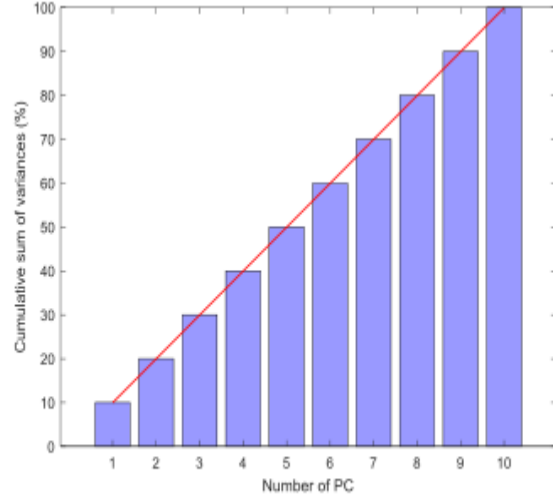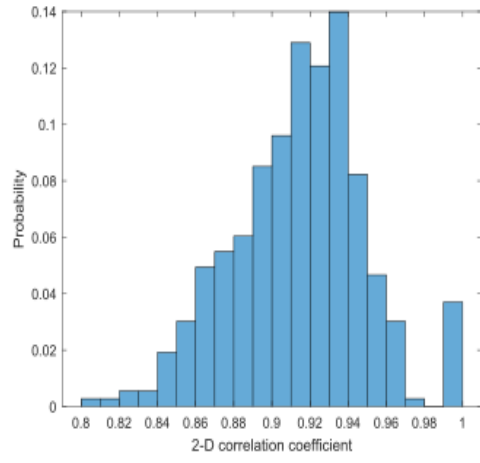|	l1 r1 s0	l1 r1 s1	l1 r1 s2	l1 r2 s0	l1 r2 s1	l1 r2 s2	l1 r0 s0	l1 r0 s1	l1 r0 s2	l2 r1 s0	l2 r1 s1	l2 r1 s2	l2 r2 s0	l2 r2 s1	l2 r2 s2	l2 r0 s0	l2 r0 s1	l2 r0 s2	l0 r1 s0	l0 r1 s1	l0 r1 s2	l0 r2 s0	l0 r2 s1	l0 r2 s2	l0 r0 s0	l0 r0 s1	l0 r0 s2
l1r1s0	1	0.96	0.92	0.95	0.95	0.96	0.97	0.93	0.95	0.95	0.93	0.91	0.90	0.93	0.92	0.88	0.93	0.93	0.93	0.90	0.94	0.87	0.93	0.91	0.93	0.94	0.94
l1r1s1		1	0.94	0.97	0.97	0.97	0.98	0.95	0.96	0.97	0.95	0.93	0.91	0.94	0.94	0.90	0.95	0.94	0.94	0.91	0.96	0.89	0.95	0.92	0.95	0.96	0.95
l1r1s2			1	0.93	0.93	0.93	0.94	0.91	0.93	0.93	0.92	0.89	0.87	0.90	0.90	0.86	0.91	0.91	0.91	0.90	0.92	0.85	0.92	0.89	0.91	0.92	0.91
l1r2s0				1	0.96	0.93	0.97	0.94	0.96	0.96	0.94	0.92	0.90	0.94	0.93	0.89	0.94	0.94	0.94	0.91	0.95	0.88	0.94	0.92	0.94	0.95	0.94
l1r2s1					1	0.96	0.97	0.95	0.96	0.96	0.94	0.92	0.90	0.94	0.93	0.89	0.94	0.94	0.94	0.91	0.95	0.88	0.94	0.92	0.94	0.95	0.94
l1r2s2						1	0.97	0.94	0.96	0.97	0.94	0.92	0.90	0.94	0.94	0.89	0.94	0.94	0.95	0.91	0.95	0.89	0.95	0.92	0.95	0.95	0.95
l1r0s0							1	0.95	0.97	0.96	0.95	0.93	0.91	0.95	0.93	0.90	0.96	0.94	0.94	0.92	0.96	0.89	0.95	0.90	0.95	0.96	0.94
l1r0s1								1	0.94	0.95	0.92	0.90	0.88	0.92	0.94	0.87	0.92	0.91	0.92	0.89	0.93	0.86	0.92	0.91	0.93	0.93	0.92
l1r0s2									1	0.96	0.94	0.92	0.91	0.95	0.94	0.91	0.94	0.93	0.94	0.90	0.95	0.89	0.94	0.90	0.95	0.96	0.94
l2r1s0										1	0.94	0.92	0.90	0.94	0.93	0.89	0.95	0.94	0.94	0.91	0.94	0.86	0.92	0.91	0.92	0.95	0.92
l2r1s1											1	0.90	0.88	0.94	0.93	0.87	0.92	0.91	0.94	0.89	0.93	0.85	0.91	0.90	0.91	0.93	0.91
l2r1s2												1	0.86	0.90	0.89	0.85	0.90	0.89	0.90	0.87	0.90	0.82	0.90	0.87	0.90	0.91	0.90
l2r2s0													1	0.87	0.87	0.87	0.93	0.88	0.87	0.84	0.84	0.85	0.89	0.89	0.88	0.90	0.88
l2r2s1														1	0.90	0.86	0.93	0.91	0.91	0.88	0.90	0.85	0.91	0.90	0.91	0.92	0.92
l2r2s2															1	0.86	0.91	0.91	0.91	0.88	0.89	0.81	0.88	0.87	0.87	0.88	0.87
l2r0s0																1	0.87	0.86	0.87	0.83	0.82	0.86	0.93	0.89	0.91	0.93	0.92
l2r0s1																	1	0.92	0.92	0.89	0.89	0.85	0.92	0.89	0.92	0.92	0.91
l2r0s2																		1	0.91	0.88	0.89	0.85	0.92	0.89	0.92	0.92	0.92
l0r1s0																			1	0.88	0.86	0.85	0.89	0.86	0.88	0.89	0.89
l0r1s1																				1	0.85	0.81	0.86	0.83	0.88	0.86	0.86
l0r1s2																					1	0.87	0.93	0.90	0.93	0.93	0.92
l0r2s0																						1	0.90	0.87	0.88	0.93	0.86
l0r2s1																							1	0.90	0.94	0.93	0.92
l0r2s2																								1	0.93	0.92	0.92
l0r0s0																									1	0.90	0.93
l0r0s1																										1	0.93
l0r0s2																											1

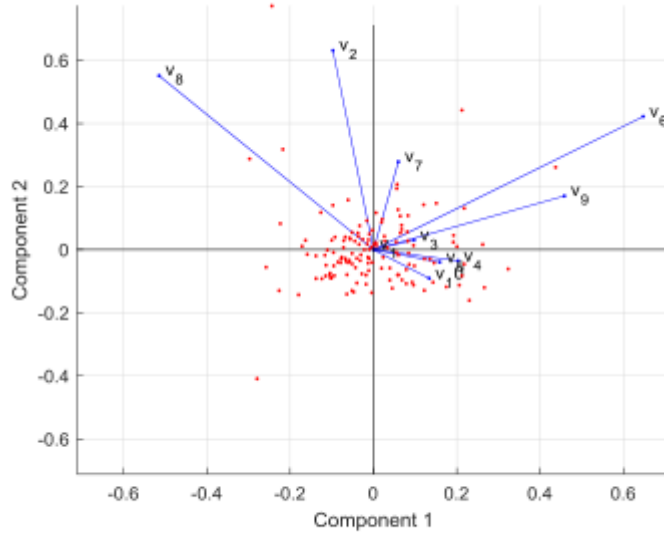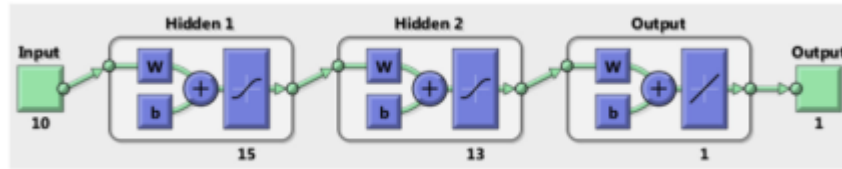**Fig. 9.** Cumulative sum of PCs variances versus the number of PCs.

Fig. 10. Loading plot of the applied principle component analysis.

Table 3
Statistical parameters of the best model for the training, test and all the data sets.

Data	MAPE (%)	MSE	R^2
Training	3.41	5.98	97.35
Test	5.10	7.31	96.93
Whole Data	3.28	5.50	97.54

2.5. Tenderness prediction

The aim of this study was to predict the beef tenderness from the image texture features obtained using the developed illumination- and affine-invariant algorithm. To this end, a Feedforward Multi-layer Perceptron (MLP) neural network was considered. The textural features extracted from each close up image (10 features) were considered as the independent variables and the tenderness value (WBSF outcome) was taken into account as dependent variable. First, the textural data were standardizes so that the mean and standard deviation of each variable were set to zero and one, respectively. Principal component analysis (PCA) was then used to map the standardized textural features to the new independent variables. Mathematically, PCA is described as an orthogonal linear transformation which transforms the data so that the first coordinate called the first principle component has the greatest variance and the second one has the second greatest variance, and so on. The full decomposition of principle components can be given by Eq. (13) as follows:

$$T = XW \quad (13)$$

where X is the standardized textural features vector, W is a matrix of weights whose columns are the eigenvectors of XTX , and T is the score vector. It is worthy to note that eigenvectors scaled up by the variances are called loadings in principal component analysis.

The scores of the PCA analysis were then fed into the neural net- work as input. The output of the MLP neural network was the tender- ness value. All the data set was divided into three groups including 65%, 10%, and 25% of all the data as the training, cross validation, and test data sets, respectively. The neural network was trained with Levenberg Marquardt learning algorithm. The MLP neural networks with one- and two-hidden layers were examined. The number of neurons in the hidden layers was considered to be in the range of 10–30. In order to eliminate the effect of initial loading of weights and biases, the developed models were trained 200 times. The performance of the developed models was evaluated using three statistical parameters, i.e., coefficient of determination ($R2$), mean absolute percentage error (MAPE), and mean of squared errors (MSE). All the procedure was carried out using the Neural Network Toolbox in MATLAB software (Release, 2016b). Matrices of the weights and biases obtained for the best neural network model have been fully provided in Appendix A.

2.6. Implementation and evaluation of smartphone app

To evaluate the tenderness of the beef samples, a new application called "BeefQuality" app was developed using Simulink programming (Appendix B) and then compiled to Java programing language with some modifications. Java Programing was conducted in Android Studio 2.0, 64 bit include Ice-cream sandwich platform (API 14), android software development kit (sdk-24.3.4), and Java development kit (jdk1.8.0_77). In addition to Java library, the OpenCV_2.4.9 was used for image processing tasks. The developed app was successfully in- stalled on an LG G4 H815 smartphone. The BeefQuality app could capture close up images from the meat sample by touching a graphical bottom embedded in the app. Once the images captured, the obtained images could be processed in real-time according to the proposed algorithm (Fig. 5) for displaying the tenderness value and the

quality percentage of the corresponding meat sample, so that the quality per- cent age of the sample with tenderness value less than 44 N was 100% (Bowling et al., 2009; Platter et al., 2003; Miller et al., 2001; Huffman et al., 1996; Shackelford et al., 1991; Savell et al., 1987) and for the sample with higher tenderness value was given via a linear relation against the tenderness value in a descending order (Eq. (14)) approved by the data of the sensory analyses reported by several studies (Miller et al., 1995, 1998; Huffman et al., 1996; Platter et al., 2003).

$$Quality\ (\%) = 3.8462\ (70 - Tenderness\ value) \qquad (14)$$

Finally, in order to validate the performance of the developed app, 30 new muscle samples were prepared and analyzed using the developed app and WBSF method. Three statistical criteria, i.e., R^2 , MSE and MAPE were used for evaluating the performance of the app.

3. Results and discussion

3.1. WBSF results

The shear force values of the beef samples were obtained using the Instron machine at the cutting edge speed of 200mm/min. The maximum shear force was the criterion for the meat tenderness. Since several cores (6 or 10) were obtained from a given beef sample, the average value of the obtained peak forces was considered as tenderness of the corresponding sample. The beef samples were categorized into tender and tough classes according to the WBSF results reported by Bowling et al. (2009). In this study, the meat quality was investigated using two parameters viz. quality percentage (%) and shear force (N). The statistical results showed that the peak shear forces for the tender samples were profoundly and significantly (p-value <0.01) lower than those of the tough samples.

3.2. Alpha value

The illumination-invariant space was determined according to Eq. (3) by having the alpha value of the image sensor. The alpha value is the weighted average of the image sensor responses to the three channels, i.e., R, G, and B. This value was computed using Eq. (4). The λi values are the peak sensitivities, giving peak response for each channel. These values could be calculated from spectral sensitivity diagram. The image sensor of the utilized smartphone was IMX2340APH5-C developed by Sony Company. According to the Spectral sensitivity diagram reported in the data sheet of the camera as shown in Fig. 6, the wavelengths related to the peak sensitivities were obtained (Table 1). Using these data, the alpha value was computed using Eq. (4).

3.3 Robustness of the developed image processing algorithm

For the sake of simplicity, herein, an image of the beef sample is denoted by I r s t i j k l which represents an image captured in the level of illumination (luminance), the level of rotation, kth level of scale, and lth level of translation. All the captured images for each beef sample were exposed to the image processing algorithm herein developed and then the 2-D correlation coefficient for each pair of the images obtained in the illumination-, rotation-, scale-, and translation invariant space were calculated. Fig. 7(a) shows a beef sample images taken in luminance of 400 lx and 700 lx, rotation of 0° and 90°, and scale of 1 and 0.8, respectively. Fig. 7(b–e) also demonstrates the corresponding illumination invariant images, the Fourier transform of the illumination invariant images, Log- Fig. 13. (a) The data reported by Miller et al. (1998) regarding the sensory tenderness rating estimated by consumers versus the WBSF values of the beef samples greater than 44 N and their linear regression model, (b) the data reported by Miller et al. (1998) about the sensory tenderness rating predicted by consumers and the tenderness acceptability (%) for the samples with WBSF values greater than 44N and their linear regression model, and (c) the data of the sensory tenderness rating and the percentage of overall acceptability for the beef samples declared by Miller et al. (1998) and their linear regression model.

Polar transform of the Fourier transform of the illumination invariant images, and the final images in the illumination-, rotation-, scale-, and translation-invariant space, respectively. The 2-D correlation coefficient for the two images in Fig. 7(e) was calculated to be 0.99 which, in turn, implies that although there was an intense difference between the two original images of the beef sample (Fig. 7(a)), the corresponding illumination- and affine-invariant images obtained through the developed algorithm were extremely similar to each other. Table 2 tabulates the 2-D correlation coefficients for the obtained images through the constructed image processing algorithm for a beef sample, for instance, at a constant level of translation (0% of the image width), three levels of luminance, three levels of rotation, and three levels of scale. The results presented in the table showed that the image processing algorithm could give the images invariant to illumination, rotation, and scale with average 2-D correlation coefficient of 0.91 with standard deviation of 0.03, demonstrating superb capability of the constructed algorithm. The probability of occurrence for the 2-D correlation coefficients resulted from analyzing the images of all the beef samples subjected to the image processing algorithm is given in Fig. 8. As can be seen in the figure, the 2-D correlation coefficients of 0.94 and 0.81 had maximum and minimum probability of occurrence, respectively. The 2-D correlation coefficient value corresponding to the center of the area for the histogram shown in Fig. 8 was approximately 0.92 and very close to the one with maximum probability which, in turn, strongly emphasized the robustness of the developed algorithm. Finally, It should be noted that statistical analysis showed non-significant effects (p-value >0.01) of illuminations, rotations, scales, translations, and replications on the 2-D correlation coefficients, indicating extraordinary capabilities of the proposed image processing algorithm.
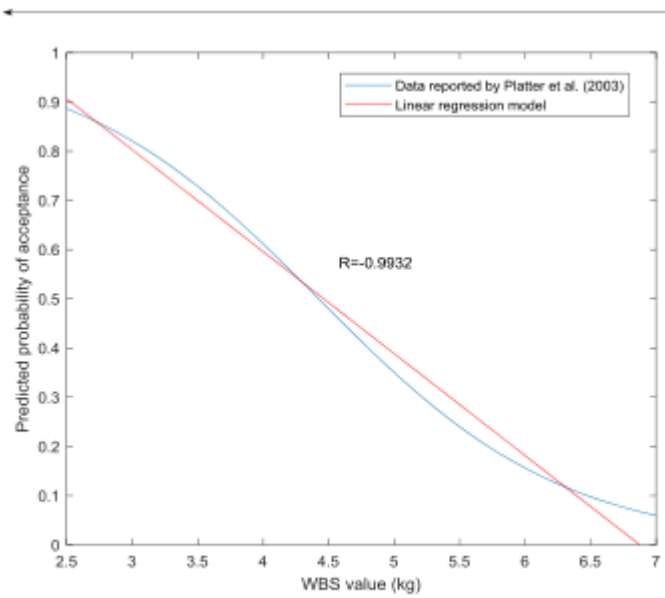
(a)

(b)

(c)

(a)

(a)

(c)
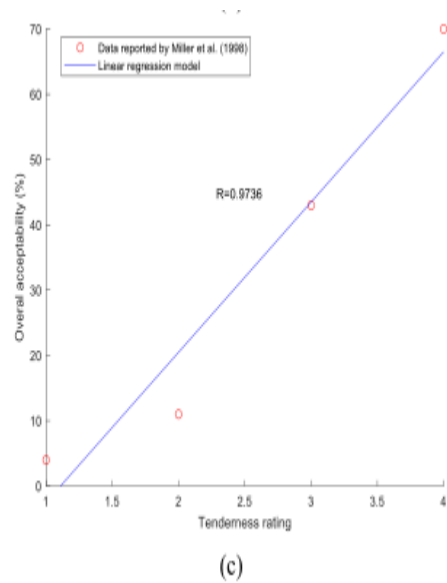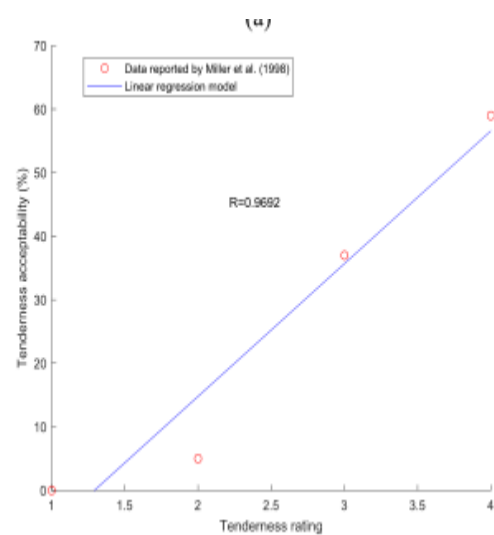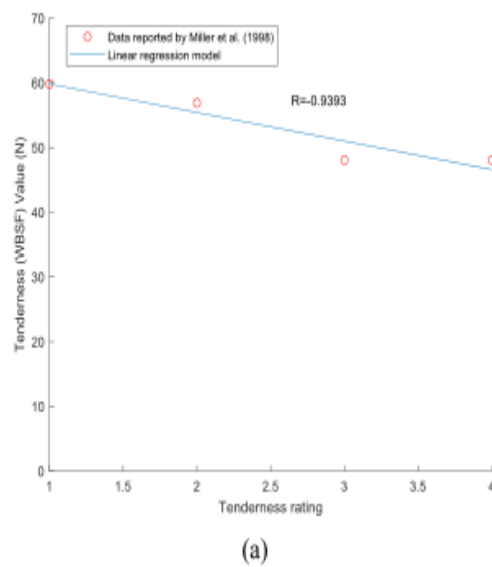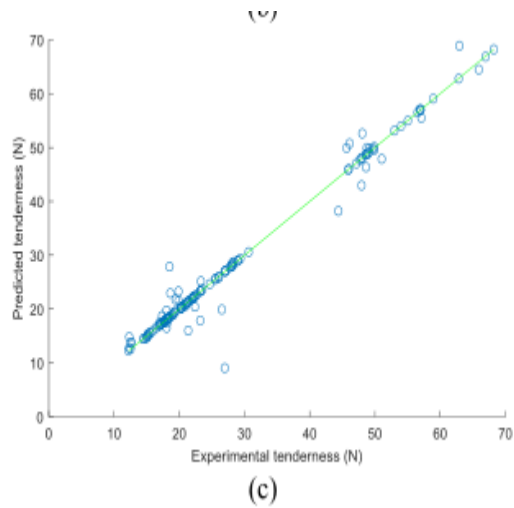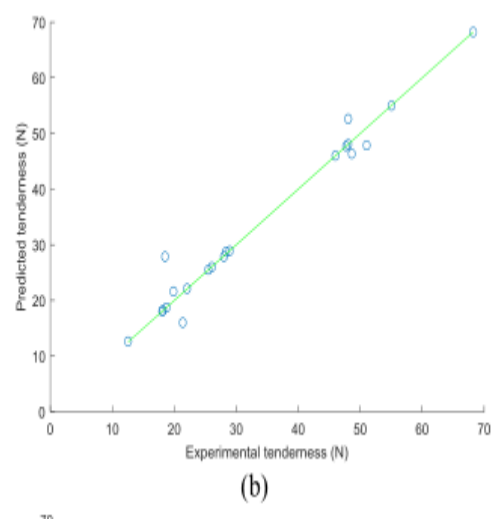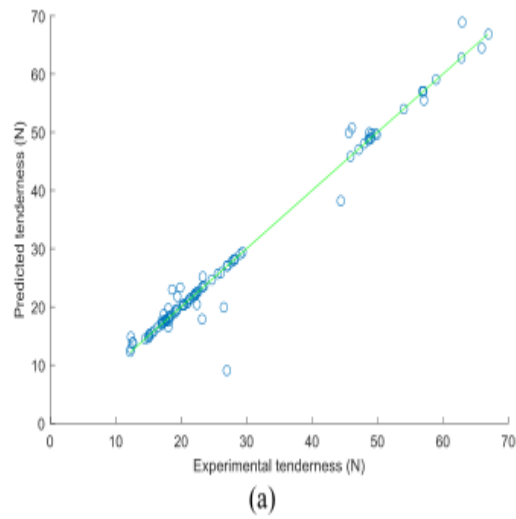
Fig. 14. The data points regarding probability of acceptance as a function of WBSF value reported by Platter et al. (2003) and their linear regression model.
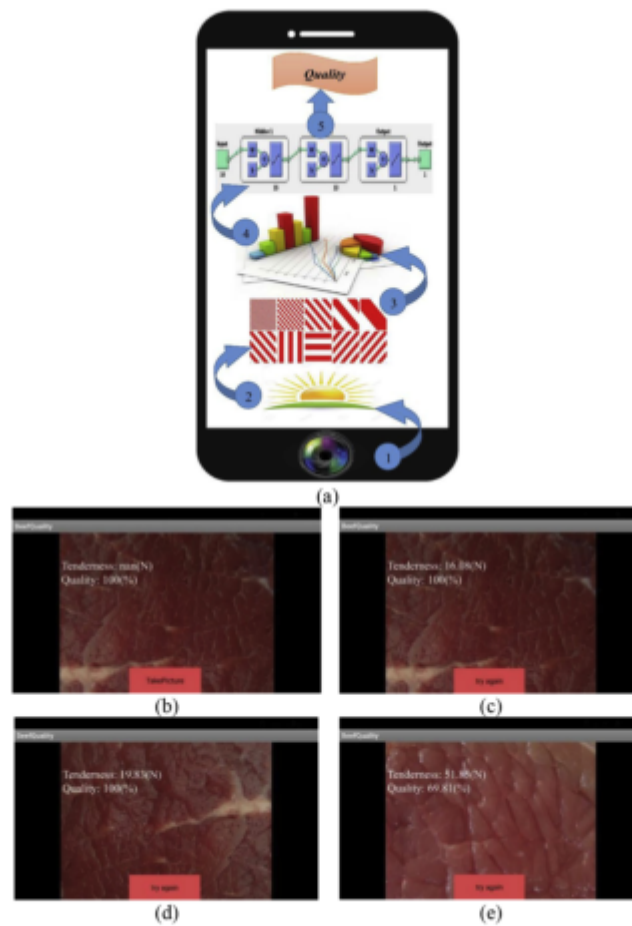

Fig. 15. (a) BeefQuality app developed on android smartphone, (b) before taking image, (c) after taking image, (d) results for a tender beef, and (e) results for a tough beef.

3.4. Principle component analysis

Fig. 9 shows the results of cumulative sum of PCs variances versus the number of PCs after transforming the standardized textural features into the new coordinate system with independent variables (PCs) using principle component analysis. As can be seen, the linear relationship between the cumulative sum of variances corresponding to the PCs and the number of PCs implies that each PC had a significant contribution to the total variances and none of them could be eliminated. Therefore, all the independent PCs were used as the inputs of the neural network model.

Loading plot of the applied principle component analysis is given in Fig. 10. All the ten variables are represented in this figure by a vector, and the direction and length of the vector indicate how each variable contributes to the first and second principal components, for example. As can be seen, the first principle component on the horizontal axis has positive coefficients almost for all the variables except for the second and eighth variables. The largest coefficient in the first principal component is the sixth, corresponding to the sixth variable. The second principle component on the vertical axis has positive coefficients for the first, second, third, sixth, seventh, eighth, and ninth variables and negative ones for the other variables. This figure also emphasized that each PC had significant contribution and could not be ignored.

3.5. ANN modeling

After some trial and error, a two-hidden layer MLP ANN model showed the best performance for predicting meat tenderness as a function of principle components. The best selected model had ten inputs, one linear neuron at the output layer, and fifteen and thirteen neurons with tangent-sigmoid transfer function in the first and second hidden layers, respectively (Fig. 11). The statistical performance parameters of the selected ANN model in the training and testing steps are summarized in Table 3. Obviously, the selected model could well predict the tenderness of the beef samples (WBSF values) with MAPE values of 3.41% and 5.10% in the training and testing steps, respectively. The MAPE value for the whole data was also found to be 3.28%. Furthermore, the coefficient of determination of the best model was about 0.97, showing the strong capability of the model for the prediction of WBSF value.

Fig. 12(a–c) shows the predicted tenderness values vs. experimental data for the training, testing, and whole datasets, respectively. It is obvious from this figure that all the data points are around a line with a slope of 45°, manifesting the fidelity and accuracy of the developed MLP ANN model.

It is worthy to note that the intelligent ANN model developed herein based on machine learning technique had ability to learn based on the experimental samples, so that the effects of the heat treatment have been automatically considered inside the ANN model and it can be said that the ANN model has learned the effects created by the heat treatment performed according to American Meat Science Association.
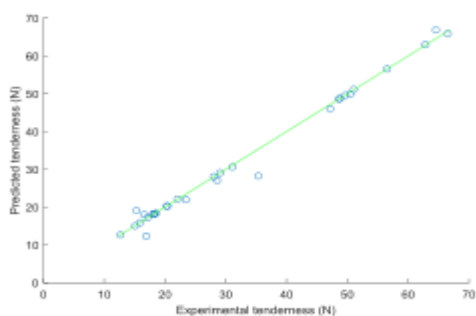
Fig. 16. WBSF values predicted by the developed app vs. experimental data obtained using the Instron machine.

3.6. WBSF value and quality percentage

To establish a relation between the WBSF value and the quality percentage (%) of the beef sample, the data regarding some sensory analyses of the beef samples reported by several authors (Miller et al., 1995, 1998; Huffman et al., 1996; Platter et al., 2003) were applied. As already mentioned, the beef sample with WBSF values less than 44N has an acceptable tenderness and can be considered as the tender sample with quality of 100% (Bowling et al., 2009; Huffman et al., 1996). Therefore, a relation should be established between the WBSF values greater than 44N and the quality percentage. Fig. 13(a) manifests the data reported by Miller et al. (1998) regarding the sensory tenderness rating estimated by consumers versus the WBSF values of the beef samples greater than 44N. As can be seen, a linear regression

model with coefficient of correlation value (R) of -0.94 could successfully fit to the data points,

indicating the superb linear relationship between tenderness rating and WBSF value. Fig. 13(b) represents the data points reported by Miller et al. (1998) about the sensory tenderness rating predicted by consumers and the tenderness acceptability (%) for the samples with WBSF values greater than 44N. As it is obvious in the figure, a linear regression model with R value of 0.97 could satisfactorily estimate the tenderness acceptability from the tenderness rating.

The data of the sensory tenderness rating and the percentage of overall acceptability (Palatability) for the beef samples declared by Miller et al. (1998) are given in Fig. 13(c). It is clear that a linear regression model with R value of 0.97 could well predict the overall acceptability (%) from the tenderness rating. The relation between probability of acceptance and WBSF values has been investigated by Platter et al. (2003). Fig. 14 illustrates the points regarding probability of acceptance as a function of WBSF value. Linear regression analysis on the data points revealed that a linear model with R value of 0.99 could satisfactorily obey the trend of the data, demonstrating the excellent linear relationship between probability of acceptance and WBSF values. It is evident from the above results that a linear relationship between WBSF values and tenderness acceptability, overall palatability (acceptability), and probability of acceptance as quality indicators of the beef samples could be well established. Therefore, in this study, a linear relationship (Eq. (14)) between quality percentage (%) and WBSF values greater than 44N was developed based on the sensory data reported by Miller et al. (1995), Miller et al. (1998), Huffman et al.(1996), and Platter et al. (2003).

19

3.7. Performance evaluation of the developed android app

Time efficiency of the developed android app was investigated on different smartphones and the results showed that the program could predict and report the tenderness value and quality percentage of a fresh beef sample in the average time duration of 1.14 (sec), indicating high efficiency of the app from the execution view point. In order to assess the reliability of the implemented android app, it was used to predict shear force value (N) and quality percentage (%) of thirty unseen beef samples as shown in Fig. 15. It should be noted that the imaging process was carried out under uncontrolled conditions in terms of illumination, rotation, translation, and scale. The results showed that the developed app could satisfactorily predict the WBSF values of the new samples with MAPE, MSE and R 2 of 3.74%, 3.34 and 0.99, respectively. The predicted tenderness values for the new samples vs. experimental data are manifested in Fig. 16. It is clear from this figure that there was an excellent agreement between the WBSF values predicted by the developed app and the experimental data obtained using the Instron machine. This, in turn, shows the adequacy and reliability of the developed app for predicting the tenderness of beef samples based on image texture features.

Li et al. (1999) predicted beef tenderness with a coefficient of determination up to 0.7 using an ANN model developed on the basis of image texture, color, and marbling, whereas the developed app, in this study, could predict the tenderness value using only the image textural features with higher coefficient of determination (R 2 = 0.9887). Xia et al. (2007) predicted beef tenderness using VIS-NIR spectral analysis with a coefficient of determination equal to 0.59, while, in the current study, an accurate prediction of beef tenderness was achieved with much higher coefficient of determination using the simpler technique namely visible image processing. Moreover, Sun et al. (2012) predicted beef tenderness using stepwise regression and support vector machine models with an accuracy close to the one obtained in the present research based on more features, i.e. color and image texture features using sophisticated instrument and technique compared with the current work. Interestingly, the developed app herein could predict beef tenderness with a coefficient of determination higher than the majority of the previously published works. It should be noted that, unlike the above-mentioned researches, the imaging process throughout this study was carried out under non-standardized and uncontrolled image acquisition conditions in terms of illumination, rotation, translation, and scale, causing the prediction of beef tenderness from fresh beef image to be more difficult. This, in turn, showed the reliability and accuracy of the proposed illumination- and affine-invariant image processing algorithm. The results obtained from the developed app further demonstrated the potential application of smartphone-based vision technology to inspect the quality of beef in real time under real-world imaging conditions.

4. Conclusion

In this study, a new Android app was developed and tested for the first time to predict the quality of fresh beef samples in real-time on the basis of images captured under real-world conditions. In order to overcome the effects of non-standardized and uncontrolled imaging

conditions, a robust illumination-, rotation-, translation-, and scale-invariant image processing algorithm was successfully developed and validated. The image texture features obtained via the developed algorithm were used to predict the experimental tenderness value (WBSF value) using an intelligent ANN model with coefficient of determination about 0.97. Once the model was successfully validated, a user-friendly app manifesting the quality percentage (%) and tenderness (WBSF) value of beef was built and deployed on an LG G4 H815 smartphone.

The developed app promisingly predicted the tenderness of thirty unseen beef samples with a coefficient of determination higher than 0.98. Therefore, this low-cost and user-friendly app can be used for accurate prediction of the beef quality in real-time under outdoor imaging conditions. Future improvements of "BeefQuality" should include the use of supplementary magnifying device to obtain images with high magnification. The accuracy of such apps could also be improved using a supplementary spectroscopic device. In addition, eliminating illumination variations using flashlight can accelerate the image processing.

Image texture analysis techniques have been greatly used in the food industry for indicating food properties and qualities. The main contribution of this study is related to image texture analysis of fresh beef samples under uncontrolled imaging conditions. Therefore, the developed app has great potential for food processing and engineering applications involving beef quality evaluation under uncontrolled conditions, so that the app can be employed by common consumers in markets or by specialists in laboratories or meat industries for beef quality evaluation. Finally, this study provides motivations to pose challenges and potential impacts for using smartphone-based vision in food engineering and processing applications.

Acknowledgement

Appendix A. Supplementary data

Supplementary data to this article can be found online at
https://doi.org/10.1016/j.jfoodeng.2018.12.009.

References

Aaslyng, M., 2002. Quality indicators for raw meat. J. Kerry D. Ledward. Meat Proc.157–174.

Asselin, D., Arsenault, H.H., 1994. Rotation and scale invariance with polar and log-polar coordinate transformations. Optic Commun. 104 (4–6), 391–404.

American Meat Science Association (AMSA), 2005. Research Guidelines for Cookery, Sensory Evaluation and Instrumental Tenderness Measurements of Fresh Meat, American Meat Science Association and National Live Stock and Meat Board. Association of Official Analytical Chemists International (AOAC), Chicago, IL, pp. 89–100 1995.

Bowling, M., Vote, D., Belk, K., Scanga, J., Tatum, J., Smith, G., 2009. Using reflectance spectroscopy to predict beef tenderness. Meat Sci. 82 (1), 1–5.

Bueno, D., Muñoz, R., Marty, J.L., 2016. Fluorescence analyzer based on smartphone camera and wireless for detection of Ochratoxin A. Sensor. Actuator. B Chem. 232, 462–468.

Casanova, C., Franco, A., Lumini, A., Maio, D., 2013. SmartVisionApp:A framework for computer vision applications on mobile devices. Expert Syst. Appl. 40 (15), 5884–5894.

Cho, S., San Park, T., Nahapetian, T.G., Yoon, J.Y., 2015. Smartphone-based, sensitive µPAD detection of urinary tract infection and gonorrhea. Biosens. Bioelectron. 74, 601–611.

Choodum, A., Kanatharana, P., Wongniramaikul, W., Daeid, N., 2013. Using the iPhone as a device for a rapid quantitative analysis of trinitrotoluene in soil. Talanta 115, 143–149.

Chung, S., Breshears, L.,E., Yoon, J., 2018. Smartphone near infrared monitoring of plant stress. Comput. Electron. Agric. 154, 93–98.

Destefanis, G., Brugiapaglia, A., Barge, M., Dal Molin, E., 2008. Relationship between beef consumer tenderness perception and Warner–Bratzler shear force. Meat Sci. 78 (3), 153–156.

ElMasry, G., Sun, D.-W., Allen, P., 2012. Near-infrared hyperspectral imaging for predicting colour, pH and tenderness of fresh beef. J. Food Eng. 110 (1), 127–140.

Fitzgerald, R., Karanassios, V., 2018. The Internet of Things (IoT) for a smartphone-enabled optical spectrometer and their use on-site and (potentially) for Industry 4.0. In: Next-generation Spectroscopic Technologies XI 2018 May 14, vol. 10657. International Society for Optics and Photonics, pp. 1065705. Han, P., Dong, D., Zhao, X., Jiao, L., Lang, Y., 2016. A smartphone-based soil color sensor: for soil type classification. Comput. Electron. Agric. 123, 232–241.

Haralick, R.M., Shanmugam, K., 1973. Textural features for image classification. IEEE Trans. Syst., Man Cybern. 6, 610–621.

Higgins, J.P., 2016. Smartphone applications for patients' health and fitness. Am. J. Med. 129 (1), 11–19.

Hosseinpour, S., Rafiee, S., Aghbashlo, M., Mohtasebi, S.S., 2014. A novel image processing approach for in-line monitoring of visual texture during shrimp drying. J. Food Eng. 143, 154–166.

Huffman, K.L., Miller, M.F., Hoover, L.C., Wu, C.K., Brittin, H.C., Ramsey, C.B., 1996. Effect of beef tenderness on consumer satisfaction with steaks consumed in the home and restaurant. J. Anim. Sci. 74, 91–97.

Hutchison, J.R., Erikson, R.L., Sheen, A.M., Ozanich, R.M., Kelly, R.T., 2015. Reagent-free and portable detection of Bacillus anthracis spores using a microfluidic incubator and smartphone microscope. Analyst 140 (18), 6269–6276.

Jabri, M. El, Abouelkaram, s., Damez, J.L., Berge, P., 2010. Image analysis study of the perimysial connective network, and its relationship with tenderness and composition of bovine meat. J. Food Eng. 96 (2), 316–322.

Jackman, P., Sun, D.W., Allen, P., Brandon, K., White, A.M., 2010. Prediction of beef palatability from colour, marbling and surface texture features of longissimus dorsi. J. Food Eng. 99 (1), 151–165.

Jacobs, S., Radnitz, C., Hildebrandt, T., 2017. Adherence as a predictor of weight loss in a commonly used smartphone application. Obes. Res. Clin. Pract. 11 (2), 206–214.

Law, R., Chan, I.C., Wang, L., 2018. A comprehensive review of mobile technology use in

hospitality and tourism. J. Hospit. Market. Manag. 27, 626–648.

Legaz, A., Verdu, R., Engan, K., 2018. Noise robust and rotation invariant framework for texture analysis and classification. Appl. Math. Comput. 335, 124–132.

Levin, S., Krishnan, S., Rajkumar, S., Halery, N., Balkunde, P., 2016. Monitoring of fluoride in water samples using a smartphone. Sci. Total Environ. 551, 101–107.

Li, J., Tan, J., Martz, F., Heymann, H., 1999. Image texture features as indicators of beef tenderness. Meat Sci. 53 (1), 17–22.

Li, J., Tan, J., Shatadal, P., 2001. Classification of tough and tender beef by image texture analysis. Meat Sci. 57 (4), 341–346.

Liao, S.C., Peng, J., Mauk, M.G., Awasthi, S., Song, J., Friedman, H., Bau, H.H., Liu, C., 2016. Smart cup: a minimally-instrumented, smartphone-based point-of-care molecular diagnostic device. Sensor. Actuator. B Chem. 229, 232–238.

Maddern, W., Stewart, A., McManus, C., Upcroft, B., Churchill, W., Newman, P., 2014. Illumination Invariant Imaging: Applications in Robust Vision-based Localisation, Mapping and Classification for Autonomous Vehicles. Proceedings of the Visual Place Recognition in Changing Environments Workshop, vol. 2. IEEE International Conference on Robotics and Automation (ICRA), Hong Kong, China, pp. 3 May 2014. Masawat, P., Harfield, A., Namwong, A., 2015. An iPhone-based digital image colorimeter for detecting tetracycline in milk. Food Chem. 184, 23–29.

Miller, M.F., Carr, M.A., Crockett, K.L., Hoover, L.C., Montgomery, J.L., Huffman, L.M., Ramsey, C.B., Wu, C.K., 1998. National beef tenderness evaluation by retail customers. Amer. Soc. of Anim. Sci., South. Sec. Abstr. 43, 12.

Miller, M.F., Carr, M.A., Ramsey, C.B., Crockett, K.L., Hoover, L.C., 2001. Consumer thresholds for establishing the value of beef tenderness. J. Anim. Sci. 79, 3062–3068.

Miller, M.F., Hoover, L.C., Cook, K.D., Guerra, A.L., Huffman, K.L., Tinney, K.S., Ramsey, C.B., Brittin, H.C., Huffman, L.M., 1995. Consumer acceptability of beef steak tenderness in the home and restaurant. J. Food Sci. 60, 963–965.

Platter, W.J., Tatum, J.D., Belk, K.E., Chapman, P.L., Scanga, J.A., Smith, G.C., 2003. Relationships of consumer sensory ratings, marling score, and shear force value to consumer acceptance of beef strip loin steaks. J. Anim. Sci. 81, 2741–2750.

Platter, W., Tatum, J., Belk, K., Koontz, S., Chapman, P., Smith, G., 2005. Effects of marbling and shear force on consumers' willingness to pay for beef strip loin steaks. J. Anim. Sci. 83 (4), 890–899.

Prieto, N., Navajas, E., Richardson, R., Ross, D., Hyslop, J., Simm, G., Roehe, R., 2010. Predicting beef cuts composition, fatty acids and meat quality characteristics by spiral computed tomography. Meat Sci. 86 (3), 770–779.

Savell, J.W., Branson, R.E., Cross, H.R., Stiffler, D.M., Wise, J.W., Griffin, D.B., Smith, G.C., 1987. National Consumer REatil Beef Study: palatability evaluations of beef loin steaks that differed in marbling. J. Food Sci. 52, 517–519.

Shackelford, S.D., Morgan, J.B., Cross, H.R., Savell, J.W., 1991. Identification of threshold levels for Warner-Bratzler shear force in beef top loin steaks. Muscle Foods 2, 289–296.

Shrivastava, S., Lee, W., Lee, N., 2018. Culture-free, highly sensitive, quantitative detection of bacteria from minimally processed samples using fluorescence imaging by smartphone. Biosens. Bioelectron. 109, 90–97.

Sun, X., Chen, K., Maddock-Carlin, K., Anderson, V., Lepper, A., Schwartz, C., Keller, W., Ilse, B., Magolski, J., Berg, E., 2012. Predicting beef tenderness using color and multispectral image texture features. Meat Sci. 92 (4), 386–393.

Swatland, H., 2006. Stratification of connective tissue toughness in beef roasts assessed by simultaneous fluorometry and penetrometry. Food Res. Int. 39 (10), 1106–1109.

Tait, R.G., 2016. Ultrasound use for body composition and carcass quality assessment in cattle and lambs. Vet. Clin. Food Anim. Pract. 32 (1), 207–218.